Dynamics of Flexible Manipulator Arms: Alternative Derivation, Verification, and Characteristics for Control

B.-S. Yuan
Nikon Precision Research Center,
Belmont, CA 94002

W. J. Book

J. D. Huggins

School of Mechanical Engineering,
Georgia Institute of Technology,
Atlanta, GA 30332

This work seeks to provide an effective way for developing the dynamics of a multi-link flexible manipulator consisting of rotary joints connecting two links. Kinematics of both the rotary joint motion and the link deformation are described by 4×4 transformation matrices as proposed in previous works (Book, 1984). The link deflection is assumed small so that the link transformation can be composed of summations of assumed link shapes. To determine the appropriate choice of component mode shapes, two essential techniques employed here are experimental and finite element methods. The resulting equations of motion allow the complete nonlinear model to be recursively derived from the Jacobian matrix and the mass properties via symbolic manipulation. Two prototype models of flexible manipulators are used to verify the dynamics with frequency and time responses. This paper contributes several new results: (1) the velocity terms (Coriolis and centrifugal forces) are related to variations in the mass matrix, (2) the skew symmetry of certain useful terms are shown, (3) the system is theoretically demonstrated to be stable with joint P.D. controllers in addition to an experimental approach, (4) practical and effective incorporation of actuator dynamics (hydraulic cylinder) and structural complexity (non-uniform cross section) is achieved through selection of mode shapes, (5) geometric constraints are incorporated through simplified coordinate transformations and (6) the results are verified on two physical cases.

I Introduction

The lightweight manipulator arm is a challenging research topic with the potential to improve the performance of robots and other high performance motion systems (Book, 1984; Bayo, 1987). The main problem with lightweight structures is in the resulting flexible vibrations naturally excited as the manipulator is commanded to move or is disturbed (Cannon and Schmitz, 1984). A suitable dynamic model is an important prerequisite for designing the flexible structure because system behavior must be predicted while improved performance is sought. Many proposed control algorithms also require dynamical models for real-time control calculation. Both the control system and mechanical system require correct models for simulation. However, the dynamical model and conventional kinematics (Asada and Slotine, 1985; Paul, 1981) that are widely used for rigid manipulators, are no longer adequate for high performance demands. Consideration of flexibility of the lightweight manipulator arm is necessary. Accuracy in the model is acquired at some cost, and the application of manipulator arms to practical endeavors gives incentive to improve the efficiency of the simulation and formulation of the dynamical models. The recursive nature of the dynamics utilized heavily in numerical formulations of models must be incorporated into symbolic manipulation via programs such as MACSYMA or SMP to reduce simulation time and eliminate the errors of manual manipulation.

In formulation of the dynamic equations of motion for the rigid-link manipulator, much work has been done (Asada and Slotine, 1985; Paul, 1981; Hollerbach, 1980) with both the Newton-Euler method and the Lagrangian method. The Newton-Euler formulation, based on the Newton's Second Law, is greatly complicated by link deflection (Greenwood, 1965). By contrast, the Lagrangian is described in terms of work and energy with generalized coordinates to develop equations of motion so that workless forces and constraint forces are not considered. The resultant equations are generally compact and provide a closed-form expression in joint torques and displacements (Asada and Slotine, 1985). By yet another alternative, Kane's method, the equations are obtained from constructing the generalized active and inertia forces with appropriate selection of the generalized speeds (Kane and Levinson, 1985).

In modeling and controlling a manipulator with a single flexible link, analysis and experimental verifications have been

Contributed by the Dynamic Systems and Control Division for publication in the JOURNAL OF DYNAMIC SYSTEMS, MEASUREMENT, AND CONTROL. Manuscript received by the Dynamic Systems and Control Division August 22, 1990; revised manuscript received July 24, 1992. Associate Technical Editor: A. G. Ulsoy.

reported (Cannon and Schmitz, 1984; Hastings, 1986). However, a single link arm has limited practical use. Some of the earliest work modeled the linear behavior of flexible arms. Book (1974) modeled multiple beams as distributed parameter systems in the frequency domain and connected them by rotary joints. Several works have modeled two flexible links (Maizza-Neto, 1974; Oakley and Cannon, 1989). Book (1) first developed the linear equations of spatial motion for a system of two rigid masses connected by a chain with an arbitrary number of massless beams and controlled joint rotations. Besides the rigid rotation of the joint, a 4×4 transformation matrix is introduced to describe the deflection of elastic elements under load. A recursive Lagrangian formulation of the dynamics of flexible manipulator arms was then obtained (Book, 1984) in which the equations are free from assumptions of a nominal motion and do not ignore the interaction of angular rates and deflections. This work extends the approach to develop the resulting equations of motion of flexible arms completely and efficiently. The elastic joint is also included. Finally, this recursive dynamics illustrates its validity through experiments on two prototype models of flexible arms.

The algorithm developed in this paper is outlined as follows. The velocity of a point on a link can be described as a linear combination of rigid body motion and flexible vibratory modes to form the kinetic energy. Two types of 4×4 transformation matrices demonstrate kinematics of the rotary joint motion and the link deformation respectively. Because of the recursive nature of the transformation chain, it is efficient to relate the position and velocity of a point in the transformation product. The potential energy of the system arises from three sources as considered here: joint elasticity, gravity and link deformation. The total kinetic and potential energy is taken into account by integrating over the entire system. Therefore, the differential equations of motion can be obtained through Lagrange's equation.

II Flexible Arm Kinematics and Kinetic Energy

2.1 Kinematics. A robot positioning task is naturally specified in Cartesian coordinates by a position vector P and a matrix of direction cosines **R**. Thus, the position of an arbitrary point attached to the rigid body can be represented as a 4×4 matrix T in a fixed coordinate system (Paul, 1981).

$$T=\begin{bmatrix} R & P \\ 0 & 1 \end{bmatrix} \tag{2.1}$$

The matrix **T** is a transformation between two coordinate systems.

In the case of flexible arms, a point along link i can be described in a coordinate system fixed to link $i-1$ by two transformations, A_i and E_i. The transformation A_i performs only joint rotation from system i' to system $i-1$ (see Fig. 2.1). The transformation E_i accounts for link length (a constant l_i) and time varying link deflection. The combined relation is

$$X_{i-1}=A_iE_iX_i \tag{2.2}$$

where

X_{i-1} = $[P_{i-1}^T, 1]^T$ = the position of the point in system $i-1$,
A_i = transformation for joint $j-1$,
E_i = transformation due to link i length and deflection.

Considering the ith consecutive coordinate transformation along a serial linkage, we can derive the location r_i of a point along the ith coordinate viewed from the base frame.

$$r_i=T_i\,{}^ir_i' \tag{2.3a}$$

where

$$T_i=A_1E_1A_2E_2\ \ldots\ A_{i-1}E_{i-1}A_i$$

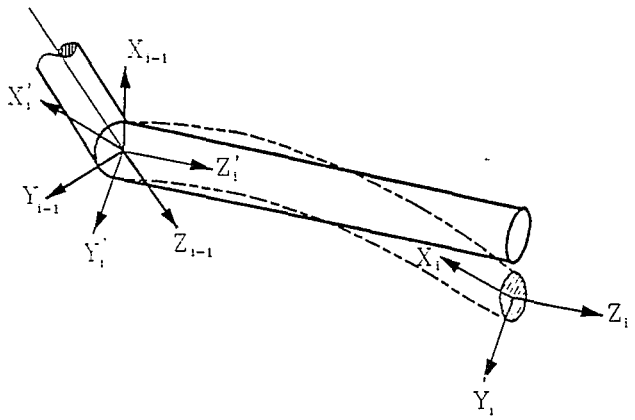

Fig. 2.1 Transformation due to rigid rotation and link deflection

and ${}^ir_i'$ is the position vector related to the ith coordinate before the transformation due to the link E_i (also see (Book, 1984)).

The transformation A_i is a function of the joint displacement q_i. Only rotational joints are allowed here. The flexible deflection is assumed to be a finite series of separable modes which are the product of admissible shape functions and time-dependent generalized coordinates. Higher modes are comparatively small in amplitude. With small deflections at the end of the link, the matrix E_i can then be expressed as

$$E_i=\sum_{j=1}^{m}\delta_{ij}\begin{bmatrix} 0 & -\theta_{zij} & \theta_{yij} & u_{ij} \\ \theta_{zij} & 0 & -\theta_{xij} & v_{ij} \\ -\theta_{yij} & \theta_{xij} & 0 & w_{ij} \\ 0 & 0 & 0 & 0 \end{bmatrix} + \begin{bmatrix} 1 & 0 & 0 & 0 \\ 0 & 1 & 0 & 0 \\ 0 & 0 & 1 & l_i \\ 0 & 0 & 0 & 1 \end{bmatrix} \tag{2.4}$$

where

δ_{ij} is the time-dependent amplitude of mode j of link i,
θ_{xij}, θ_{yij}, and θ_{zij} are the angles of rotation about x, y, and z, respectively, of mode i of link j
u_{ij}, v_{ij}, and w_{ij} are the deflection components of mode j of link i, in x, y, and z directions, respectively
m_i is the number of modes used to describe the deflection of link i,
l_i is the length of link i.

Note, if the point in question is not at the end of the link, replace l_i with z_i measured to that point.

2.2 Kinetic Energy. In this section, the expression for the system kinetic energy is developed for use in Lagrange's equations. First, consider the kinetic energy of a point on the ith link:

$$KE_i=\int_{\text{link}_i} dKE_i=\frac{1}{2}\int_{\text{link}_i}\text{Trace}\left(\frac{dr_i}{dt}\frac{dr_i^T}{dt}\right)dm \tag{2.5}$$

where dr_i/dt is called the velocity vector, and from (2.3a)

$$\frac{dr_i}{dt}=\dot{T}_i\,{}^ir_i+T_i\,{}^i\dot{r}_i \tag{2.6}$$

Equation (2.5) becomes

$$KE_i=\frac{1}{2}\int_{\text{link}_i}\text{Trace}\left(\dot{T}_i\,{}^ir_i\,{}^ir_i^T\dot{T}_i^T+2\dot{T}_i\,{}^ir_i\,{}^i\dot{r}_i^TT_i^T + T_i\,{}^i\dot{r}_i\,{}^i\dot{r}_i^TT_i^T\right)dm \tag{2.7}$$

Summing over all n links, one finds the system kinetic energy to be

$$KE=\sum_{i=1}^{n}\int_{\text{link}_i} dKE_i \tag{2.8}$$

$$KE=\sum_{i=1}^{n}\text{Trace}\,(\dot{T}_iB_{3i}\dot{T}_i^T+2\dot{T}_iB_{2i}T_i^T+T_iB_{1i}T_i^T) \tag{2.8b}$$

where

$$B_{1i}=\sum_{j=1}^{m_i}\sum_{k=1}^{m_i}\dot{\delta}_{ij}\dot{\delta}_{ik}C_{ikj} \tag{2.8c}$$

$$C_{ikj}=\frac{1}{2}\int_{\text{link}_i}[u_{ik},v_{ik},w_{ik},0]^T[u_{ij},v_{ij},w_{ij},0]dm \tag{2.8d}$$

$$B_{2i}=\sum_{j=1}^{m_i}\dot{\delta}_{ij}C_{ij}+\sum_{k=1}^{m_i}\sum_{j=1}^{m_i}\delta_{ik}\dot{\delta}_{ij}C_{ikj} \tag{2.8e}$$

$$C_{ij}=\frac{1}{2}\int_{\text{link}_i}[0,0,z_i,1]^T[u_{ij},v_{ij},w_{ij},0]dm \tag{2.8f}$$

$$B_{3i}=C_i+\sum_{j=1}^{m_i}\delta_{ij}[C_{ij}+C_{ij}^T]+\sum_{k=1}^{m_i}\sum_{j=1}^{m_i}\delta_{jk}\delta_{ij}C_{ikj} \tag{2.8g}$$

$$C_i=\frac{1}{2}\int_{\text{link}_i}[0,0,z_i,1]^T[0,0,z_i,1]dm \tag{2.8h}$$

Note that $dm = Mdz_i$ for a slender beam i, M is density/area. (2.8h) contains the rigid body inertia term for link i.

It should be mentioned that the kinetic energy for rigid robotic arms can be obtained with the same procedure without considering link deflection (Paul, 1981), and the steps leading to these terms are found in the reference (Book, 1984). Equations (2.8e) and (2.8g) are also redefined as

$$B_{2i}=\sum_{j=1}^{m_i}\dot{\delta}_{ij}\left(C_{ij}+\sum_{k=1}^{m_i}\delta_{ij}C_{ikj}\right)=\sum_{j=1}^{m_i}\dot{\delta}_{ij}D_{ij} \tag{2.9a}$$

$$B_{3i}=C_i\sum_{j=1}^{m_i}\delta_{ij}\left[(C_{ij}+C_{ij}^T)+\sum_{k=1}^{m_i}\delta_{ik}C_{ikj}\right]=F_i \tag{2.9b}$$

Alternatively, the kinetic energy can be expressed by

$$KE=\frac{1}{2}\dot{X}^TM\dot{X}=\frac{1}{2}\sum_{i=1}^{n}\sum_{j=0}^{m_i}\sum_{\alpha=1}^{n}\sum_{\beta=0}^{m_\alpha}m_{ij\alpha\beta}\dot{X}_{ij}\dot{X}_{\alpha\beta} \tag{2.10a}$$

where

$m_{ij\alpha\beta}$ are the elements of the inertia matrix $\mathbf{M}$,

$\dot{X}_{ij}$ is the velocity vector including all generalized velocities, $\dot{q}_i$ and $\dot{\delta}_{ij}$, and let

$$X_{ij}=\begin{cases}q_i & j=0\\ \delta_{ij} & j=1,2,\ \ldots,\ m_i\end{cases} \tag{2.10b}$$

To equate (2.8b) and (2.10a), first let the derivative of T_i with respect to time be

$$\dot{T}_i=\sum_{h=1}^{i}\hat{T}_{h-1}U_h{}^h\bar{T}_i\dot{q}_h+\sum_{h=1}^{i-1}\sum_{k=1}^{m_i}T_hN_{hk}{}^hT_i\dot{\delta}_{hk} \tag{2.11a}$$

where

$$U_h=\frac{\partial A_h}{\partial q_h} \tag{2.11b}$$

$$N_{hk}=\begin{bmatrix}0 & -\theta_{zhk} & \theta_{yhk} & u_{hk}\\ \theta_{zhk} & 0 & -\theta_{xhk} & v_{hk}\\ -\theta_{yhk} & \theta_{xhk} & 0 & w_{hk}\\ 0 & 0 & 0 & 0\end{bmatrix} \tag{2.11c}$$

$$\hat{T}_{h-1}=A_1E_1\ \ldots\ A_{h-1}E_{h-1} \tag{2.11d}$$

$$h\bar{T}_i=E_hA_{h+1}\ \ldots\ E_{i-1}A_i \tag{2.11e}$$

Then, through exchanging the trace and sum operation and collecting the terms along with arranging them for efficient computation, the inertia coefficients in (2.10a) are divided into three groups: the joint angles $\dot{q}_i\dot{q}_j$, the joint angle and link deflection $\dot{q}_i\dot{\delta}_{ij}$ and the link deflections $\dot{\delta}_{ij}\dot{\delta}_{\alpha\beta}$.

All occurrences of $\dot{q}_i\dot{q}_j$ are in the first term of the right-hand side of Eq. (2.8b)

$$\frac{1}{2}\sum_{i=1}^{n}\sum_{\alpha=1}^{i}\sum_{h=1}^{i}\text{Trace}[(\hat{T}_{\alpha-1}U_\alpha{}^\alpha\bar{T}_i)F_i(\hat{T}_{h-1}U_h{}^hT_i)^T]\dot{q}_\alpha\dot{q}_h \tag{2.12a}$$

However, the inertia coefficients of $\dot{q}_h\dot{\delta}_{ij}$ come from the first and second terms of Eqs. (2.8b) and are shown as

$$\frac{1}{2}\sum_{i=1}^{n}\sum_{h=1}^{i}\left\{\sum_{\alpha=1}^{i-1}\sum_{\beta=1}^{m_\alpha}\text{Trace}[(\hat{T}_{h-1}U_h{}^h\bar{T}_i)F_i(T_\alpha N_{\alpha\beta}{}^\alpha\hat{T}_i)^T]\dot{q}_h\dot{\delta}_{\alpha\beta}+\sum_{j=1}^{m_i}2\,\text{Trace}[(\hat{T}_{h-1}U_h{}^hT_{h-1})D_{ij}T_i^T]\dot{q}_h\dot{\delta}_{ij}\right\} \tag{2.12b}$$

The three terms of the right-hand side of Eq. (2.8b) which include $\dot{\delta}_{ij}\dot{\delta}_{\alpha\beta}$ are expressed as follows:

$$\frac{1}{2}\sum_{i=1}^{n}\left\{\sum_{h=1}^{i-1}\sum_{k=1}^{m_h}\left(\sum_{\alpha=1}^{i-1}\sum_{\beta=1}^{m_\alpha}\text{Trace}[(T_hN_{hk}{}^h\hat{T}_i)F_i(T_\alpha N_{\alpha\beta}{}^\alpha\hat{T}_i)^T]\dot{\delta}_{ik}\dot{\delta}_{\alpha\beta}+2\,\text{Trace}[(T_hN_{hk}{}^h\hat{T}_i)D_{ik}T_i^T]\dot{\delta}_{hk}\dot{\delta}_{ij}\right)+\sum_{j=1}^{m_i}\sum_{k=1}^{m_i}\text{Trace}[T_iC_{ikj}T_i^T]\dot{\delta}_{ij}\dot{\delta}_{ik}\right\} \tag{2.12c}$$

Those terms (2.12) also appear in (Book, 1984).

III System Potential Energy

In addition to the computation of the kinetic energy, we need to find the potential energy in order to derive Lagrange's equations of motion for the dynamic system. The potential energy of the system includes three sources: joint elasticity, gravity and link deformation. The first term is associated with joint coordinates q, the second term is a function of position, and the last term, called the strain energy, results from the energy stored in the link due to deformation. The potential energy related to the gravity and link deflection can be obtained from integrating over the length of the individual link, and then summing over all links.

3.1 Elastic Joint Potential Energy. We consider an n-link manipulator with revolute joints, and model the elasticity of the ith joint as an equivalent torsional spring with stiffness K since each kinematic joint is actuated directly with some sort of actuator. However, for a linear actuator used to rotate a revolute joint through the use of a four-bar linkage, the equivalent stiffness can be found by the corresponding transformation between joint and actuator spaces (Spong, 1987).

The coordinate $\bar{q}_i$ in the joint transformation A_i along with the equivalent stiffness K_{ei} constitutes the elastic joint potential energy which does not involve the coordinates associated with link deflections. The formula for this potential energy is described as

$$PE_e=\sum_{i=1}^{n}PE_{ei}=\sum_{i=1}^{n}\frac{1}{2}K_{ei}\bar{q}_i^2 \tag{3.1a}$$

The coordinate $\bar{q}_i$ is measured from the unstretched position

to q_i. In other words, the elastic joint potential energy has the positive value relative to the "basic energy" which is a function of the unstretched position.

3.2 Gravity Potential Energy. In robotic arms with elasticity, the gravity potential energy for a differential element on the ith link is

$$dPE_{gi} = -g^T T_i{}^i r_i dm \tag{3.2a}$$

where the gravity vector g has the form

$$g^T = [g_x, g_y, g_z, 0] \tag{3.2b}$$

Integrating over the link and summing over all links, the gravity potential energy becomes

$$PE_g = -g^T \sum_{i=1}^{n} T_i h_i \tag{3.3a}$$

where

$$h_i = M_i h_{mi} + \sum_{k=1}^{m_i} \delta_{ik} \epsilon_{ik}$$

M_i = the total mass of link i,

$h_{mi} = [0, 0, h_{zi}, 1]^T$ = a vector to the center of gravity from joint i (undeformed).

$$\epsilon_{ik} = \int_{\text{link}_i} [u_{ik}, v_{ik}, w_{ik}, 0]^T dm \tag{3.3c}$$

From the above equations, we know that if the link is homogeneous, the total distance to the center of gravity is the vectoral sum of the deformed and undeformed parts. However, the gravity potential energy is a function of generalized coordinates q_i and δ_{ij}.

3.3 Link Strain Potential Energy. The link deflection for a slender beam is assumed to be a linear combination of the generalized coordinates $\delta_{ik}(t)$ and mode shapes u_{ik}, v_{ik}, and w_{ik} in x, y, and z axes respectively, while the rotational components of the link deflection are taken into account in the z axis. Compression w_{ik} is not initially included as it is generally much smaller. With a truncated modal approximation for the ith link deformation, the equation in the x-direction is shown as

$$u_{xi} = \sum_{k=1}^{m_i} \delta_{ik} u_{ik} \tag{3.4a}$$

v_{yi} is similarly represented in the y-direction and

$$\theta_{zi} = \sum_{k=1}^{m_i} \delta_{ik} \theta_{zik} \tag{3.4b}$$

The strain potential energy related to the link deformation which is integrated along the z-axis coincident with the link is described as

$$PE_{di} = \frac{1}{2} \int_{\text{link}_i} \left[EI_x \left(\frac{\partial^2 u_{xi}}{\partial z_i^2} \right)^2 + EI_y \left(\frac{\partial^2 v_{yi}}{\partial z_i^2} \right)^2 + E_G J_z \left(\frac{\partial \theta_{zi}}{\partial z_i} \right)^2 \right] dz_i \tag{3.5}$$

where E is Young's modulus of elasticity, and I_x and I_y are the area moments of the inertia of the link about an axis parallel to the x and y axes, respectively, and through the centroid of the cross section. E_G is the shear modulus and J_z is the polar area moment of inertia of the link about the centroid.

Substituting (3.4) into (3.5), PE then becomes

$$PE_{di} = \frac{1}{2} \sum_{j=1}^{m_i} \sum_{k=1}^{m_i} \delta_{ij} \delta_{ik} (K_{xijk} + K_{yijk} + K_{zijk}) \tag{3.6a}$$

where K_{xijk}, K_{yijk}, and K_{zijk} are stiffness coefficients,

$$K_{xijk} = \int_{\text{link}_i} EI_x \frac{d^2 u_{ij}}{dz_i^2} \frac{d^2 u_{ik}}{dz_i^2} dz_i \tag{3.6b}$$

$$K_{yijk} = \int_{\text{link}_i} EI_y \frac{d^2 v_{ij}}{dz_i^2} \frac{d^2 v_{ik}}{dz_i^2} dz_i \tag{3.6c}$$

$$K_{zijk} = \int_{\text{link}_i} E_G J_z \frac{d\theta_{zij}}{dz_i} \frac{d\theta_{zik}}{dz_i} dz_i \tag{3.6d}$$

Note that the stiffness coefficient matrix is symmetric, for example, $K_{xijk} = K_{xikj}$. The link potential energy for the total system PE can therefore be written as

$$PE_d = \frac{1}{2} \sum_{i=1}^{n} \sum_{j=1}^{m_i} \sum_{k=1}^{m_i} \delta_{ij} \delta_{ik} K_{dijk} \tag{3.7}$$

where $K_{dijk} = K_{xijk} + K_{yijk} + K_{zijk}$.

PE_d is independent of q_i, the joint coordinate. In fact, Eq. (3.7) can be made much more general than the initial assumptions regarding the link strain energy. Compression strain energy and link forms other than beam, for example, can also be represented in this formulation. The values of coefficients K_{dijk} are determined analytically or numerically, e.g., by finite element methods. Combining elastic joint and link strain energies leads to

$$PE_e + PE_d = \frac{1}{2} \sum_{i=1}^{n} \sum_{j=1}^{m_i} \sum_{k=1}^{m_i} K_{ijk} \bar{X}_{ij} \bar{X}_{ik} \tag{3.8}$$

where

$$\bar{X}_{ij} = \begin{cases} \bar{q}_i & j = 0 \\ \delta_{ij} & j = 1, 2, \ldots, m_i \end{cases}$$

IV Equations of Motion

The Lagrangian formulation shown as below results in a compact system of equations which is appealing from both the dynamic modeling and control engineering points of view.

$$\frac{d}{dt}\left(\frac{\partial KE}{\partial \dot{x}}\right) - \frac{\partial KE}{\partial x} + \frac{\partial PE}{\partial x} = Q \tag{4.1}$$

where Q is the generalized force corresponding to joint variable q. For the deflection variables, the corresponding generalized force will be zero if the corresponding modal deflection or rotations have no displacement at those locations where external forces or moments are applied. Thus, it is assumed for the present development that the modal functions are selected so that is the case. This is convenient for utilizing the result as well since joint angle sensors measure the variable q.

Since $m_{ij\alpha\beta}$ is a function of x_{ij} or $x_{\alpha\beta}$ in (2.10a), the first term in (4.1) is computed as

$$\frac{d}{dt}\left(\frac{\partial KE}{\partial \dot{x}}\right) = \frac{d}{dt}\left(\sum_{i=1}^{n} \sum_{j=0}^{m_i} m_{ijpq} \dot{x}_{ij}\right)$$

$$= \sum_{i=1}^{n} \sum_{j=0}^{m_i} m_{ijpq} \ddot{x}_{ij} + \sum_{i=1}^{n} \sum_{j=0}^{m_i} \frac{dm_{ijpq}}{dt} \dot{x}_{ij}$$

$$= \sum_{i=1}^{n} \sum_{j=0}^{m_i} m_{ijpq} \ddot{x}_{ij} + \sum_{i=1}^{n} \sum_{j=0}^{m_i} \sum_{\alpha=1}^{n} \sum_{\beta=0}^{m_\alpha} \frac{\partial m_{ijpq}}{\partial x_{\alpha\beta}} \dot{x}_{ij} \dot{x}_{\alpha\beta} \tag{4.2}$$

The second term in (4.1) includes the partial derivative of the kinetic energy given by

$$\frac{\partial KE}{\partial x_{pq}} = \frac{\partial}{\partial x_{pq}}\left(\frac{1}{2} \sum_{i=1}^{n} \sum_{j=0}^{m_i} \sum_{\alpha=1}^{n} \sum_{\beta=0}^{m_\alpha} m_{ij\alpha\beta} \dot{x}_{ij} \dot{x}_{\alpha\beta}\right)$$

$$= \frac{1}{2} \sum_{i=1}^{n} \sum_{j=0}^{m_i} \sum_{\alpha=1}^{n} \sum_{\beta=0}^{m_\alpha} \frac{\partial m_{ij\alpha\beta}}{\partial x_{pq}} \dot{x}_{ij} \dot{x}_{\alpha\beta} \tag{4.3}$$

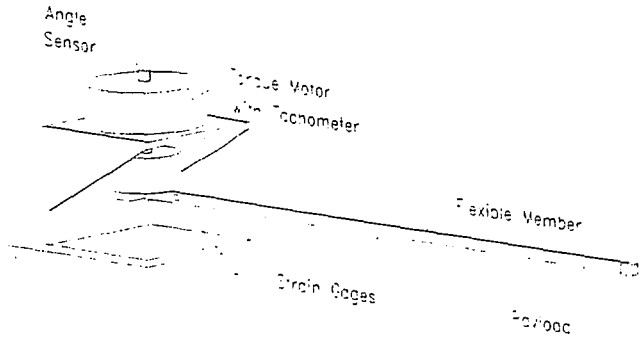

Fig. 5.1 Single Link flexible Manipulator (SLIM)

Table 5.1 Physical properties of one-link flexible manipulator

Aspect	System value
Material	—Aluminum 6061-T6
Form	—Rectangular 3/4 × 3/16 in.
Length	—48 in.
Moment of Inertia	—4.12E-4 in. 4
EI Product	—4120 lbf-in. 4

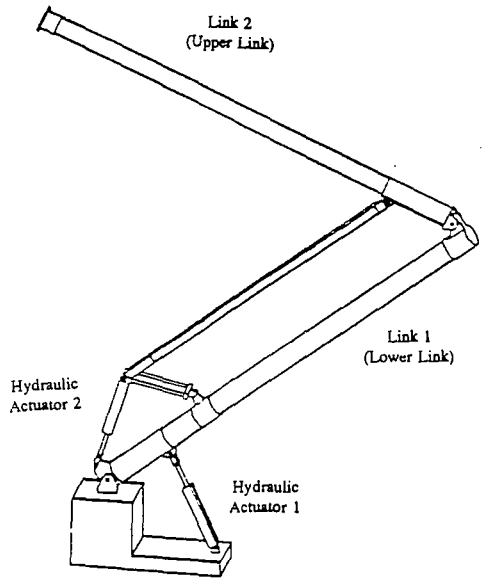

Fig. 5.2 RALF (Robotic Arm, Large, and Flexible)

Taking the partial derivative of the potential energies of the elastic joint and the link deflection leads to

$$\frac{\partial (PE_e + PE_d)}{\partial x_{pq}} = \sum_{l=0}^{m_i} K_{piq} \bar{x}_{pl} \tag{4.4}$$

And the gravity term comes from (3.3)

$$\frac{\partial PE_g}{\partial x_{pq}} = \begin{cases} -g^T \sum_{i=p}^{n} \frac{\partial T_i}{\partial x_{pq}} h_i - gTT_p \epsilon_{pq} & \text{when } q \neq 0 \\ -g^T \sum_{i=p}^{n} \frac{\partial T_i}{\partial x_{pq}} h_i & \text{when } q = 0 \end{cases} \tag{4.5}$$

Notice that

$$\sum_{i=p}^{n} \frac{\partial T_i}{\partial x_{pq}} = \frac{\partial A_n}{\partial q_n} = 0$$

when $p = n$ and $q = 0$. Hence, the gravity term is a function of x and we define $G(X) = [G_{pq}]$ with elements (4.5).

Finally, substituting (4.2), (4.3), (4.4), and (4.5) into (4.1), we can obtain the equations of motion affected by Q_{pq}

$$\sum_{i=1}^{n} \sum_{j=0}^{m} m_{ijpq} \ddot{x}_{ij} + \sum_{i=1}^{n} \sum_{j=0}^{m} \sum_{\alpha=1}^{n} \sum_{\beta=0}^{m_i} C_{ij\alpha\beta pq} \dot{x}_{ij} \dot{x}_{pq} + \sum_{l=0}^{m_i} K_{plq} x_{pl} + G_{pq} = Q_{pq} \tag{4.6a}$$

where

$$C_{ij\alpha\beta pq} = \frac{\partial m_{ijpq}}{\partial x_{\alpha\beta}} - \frac{1}{2} \frac{\partial m_{ij\alpha\beta}}{\partial x_{pq}} \tag{4.6b}$$

The dynamic Eq. (4.6a) can also be written in matrix-vector form as

$$M(X)\ddot{X} + H(X,\dot{X})\dot{X} + K\bar{X} + G(X) = Q \tag{4.7}$$

where $H(X, \dot{X})\dot{X} = C(X, \dot{X})$ and $C_{ij\alpha\beta pq}$ is the element's coefficient of C (Appendix A). More detail in C can be found in (Book, 1984). Equation (4.6b) is claimed to be an effective equation to generate C using a symbolic program when the inertia matrix is known.

Conclusively, the element of the inertia matrix $M(X)$ arises from Eq. (2.12). The coupling elements are from (4.6b). The stiffness matrix K is determined by the elastic joint and the link deflection energies (3.8) or (4.4). Appendix A illustrates that the inertia matrix is positive definite as well as symmetric, and (M-2H) is skew-symmetric. For further work of controlling the dynamic system of flexible manipulators, the joint PD controllers, which have exhibited adequate control performance for rigid robotic manipulators (Asada and Slotine, 1985) also theoretically demonstrate stability for flexible manipulators (Appendix B).

V Experimental Setups

Two prototype models of flexible robotic arms at the Flexible Automation Laboratory at Georgia Tech are used to verify the dynamic equations derived in the previous sections. The frequency and time responses are two approaches that can be used to demonstrate agreement between analytical and experimental results. The actuator dynamics will be considered because it is presented in the experimental systems. However, a linear case has been adapted for comparing analytical and experimental results, using sufficiently slow and small motion of the links.

The first experimental apparatus (Fig. 5.1) is a one-link flexible manipulator driven by an electric torque motor. The arm is a four foot aluminum beam with the section oriented so that there is increased flexibility in the horizontal plane. Two strain gages mounted at the base and at mid-length of the beam measure the link deflection. Table 5.1 lists the physical properties (Hastings, 1986).

The other apparatus is a two link manipulator, RALF (Robotic Arm, Large, and Flexible), with a parallel mechanism (Fig. 5.2). Each link is a cylindrical hollow beam, ten feet long. The parallel mechanism's function is force transmission for actuating the upper link. The weight of the robotic structure is about seventy pounds. More details are given in the paper by Huggins (1988). The analytical work involved is more complicated than the first case.

VI The Case of a One-Link Flexible Manipulator

The process of forming the dynamic model for flexible manipulators has been discussed. One difference from the rigid manipulator is the existence of the stiffness term in (4.7) which determines the system vibration due to the flexible link deflection. Since the one-link beam moves only in the horizontal plane, the flexible deflection is simply described by an infinite series of separable modes, i.e., the deflection in x and z di-

Table 6.1 Comparison of modal frequencies (Hz) of one-link case

Mode	Measured	Analytical	Finite element
1	2.08	2.096	2.088
2	13.92	13.989	13.955
3	41.38	41.524	41.452
4	81.18	81.225	81.203
5		136.352	136.345

rection of E in (2.2) has been ignored. However, the first few modes will be accurate enough to describe the flexible deflection because the amplitudes of higher modes are small compared to the amplitudes of the lower modes. Here, n is selected to be 2 (Hastings and Book, 1987). The transformation of a rigid-body motion has been expressed as A in (2.2). Thus, the equation of motion can be derived as presented in reference (Yuan et al., 1989).

The beam, directly driven by the torque motor (which is here considered as a high bandwidth torque source), is controlled by feedback signals from the joint in the case of a one-link manipulator. Therefore, the clamped-mass boundary conditions are imposed such that the mode shapes can be derived from the Bernoulli-Euler beam formulation. Because it is a simple structure, the solution can be obtained analytically (Yuan et al., 1989). Table 6.1 compares the measured modal frequencies to those computed from the linear dynamical equations with the mode shapes using the analytical method.

When a small amount of proportional damping is employed (Meirovitch, 1967), the simulations of the dynamics motion with two modes result in the plot shown in Fig. 6.1(*a*), (*b*) for a step change in the desired joint angle. Note that joint feedback has been implemented in this case. The strain measurement at the base is shown in reference (Hastings and Book, 1987). It can be seen in Table 6.1 that the model implemented with only the first few modes produces system natural frequencies that agree to less than 1 percent with the experimental data (Hastings, 1986). Obviously, the clamped-mass shape is acceptable in representing the link deflection in this case.

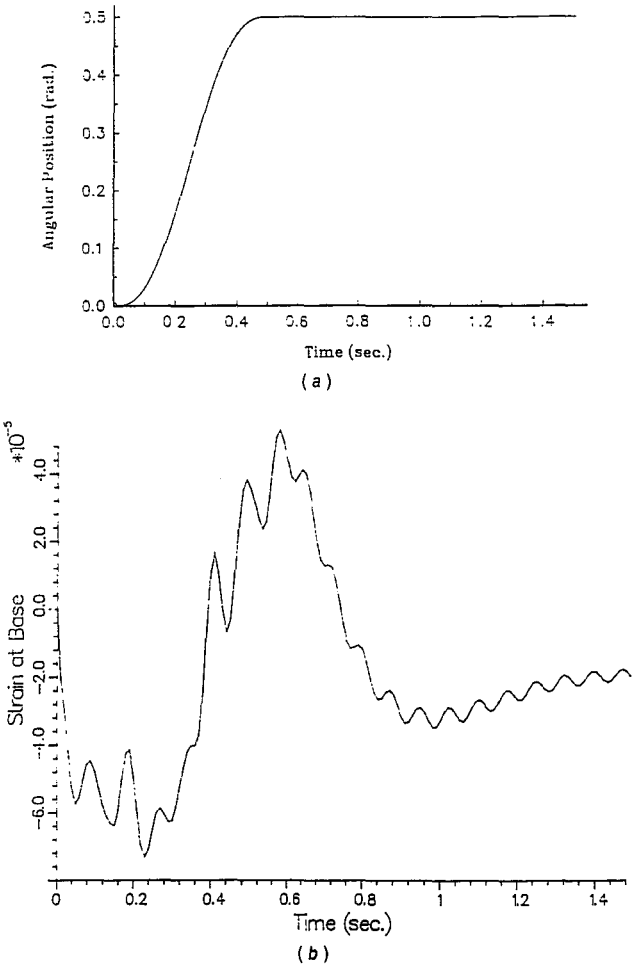

Fig. 6.1 (*a*) Simulated joint angular response, (*b*) Simulated strain response at base

VII The Case of RALF

The total system of RALF should include the actuator dynamics in addition to the two-link manipulator with a parallel mechanism. Hydraulic actuators are employed to drive the structure. Since the actuator has an equivalent stiffness as its dynamical characteristic, natural frequencies of the total system may differ from the original static system.

For this experiment, the hydraulic actuator including the servovalve and amplifier is simplified as a third order transfer function from the input voltage of the valve motor x_s to the piston displacement x_p of the hydraulic cylinder (Merritt, 1967). The hydraulic natural frequency ω_h is, therefore, obtained from the transfer function, while the hydraulic spring rate k_h is simply a useful concept in computing hydraulic natural frequencies and interpreting dynamic response. By imposing a swept sine input and using an LVDT (linear variable-differential transformer) attached to the piston rod to measure the displacement data, the frequency response tests for the joint 1 and 2 actuators were performed. No load was placed on the actuators. Curve fitting the measured frequency response data, the transfer functions are:

$$\text{For actuator 1: } \frac{x_p}{x_s} = \frac{5.217E3}{S(S^2 + 3.836E2S + 7.509E4)} \quad (7.1a)$$

$$\text{For actuator 2: } \frac{x_p}{x_s} = \frac{3.374E3}{S(S^2 + 4.838E2S + 9.869E4)} \quad (7.1b)$$

The hydraulic natural frequencies for the actuators at 1 and 2 are approximately 43.6 Hz and 50.0 Hz. Thus, the hydraulic spring rates are calculated to be $1.54E3$ lb/in for actuator 1 and $6.03E3$ lb/in for actuator 2.

Experimental mode shapes are observed from the frequency functions. The excitation consisted of a swept sine wave. Measurements were taken by accelerometers sequentially placed along the link at 10 points on each link. The deflection amplitude is then obtained by integrating the acceleration spectrum twice. A cubic spline is used to connect the amplitude values at discrete points to obtain the curves in Fig. 7.1 through 7.4. Note that a third order polynomial is the lowest order that can satisfy the Bernoulli-Euler equation for continuity of bending moments.

7.1 Finite Element Method for Modeling RALF. From the previous sections, we recognize that the link deflection is the main component of system oscillation for the flexible manipulator. However, the clamped-mass mode shapes of simple beams, which are conveniently derived analytically, may not be suitable for complicated structures like RALF. It is easily observed in Fig. 5.2 that the major difference between the RALF and two serial-link arm is a drive link parallel to the lower link (link 1) used to drive the upper link (link 2) in RALF. The parallel drive link and link 1 form a closed kinematic chain. Finite element methods are used to analyze the system and comparisons are made between the numerical and experimental results. Table 7.1 shows comparison of the results from experiments and finite element methods with the joint angle between link 1 and link 2 equal 90 degrees. Measurements are taken by a force transducer on the shaker and an accelerometer on the link.

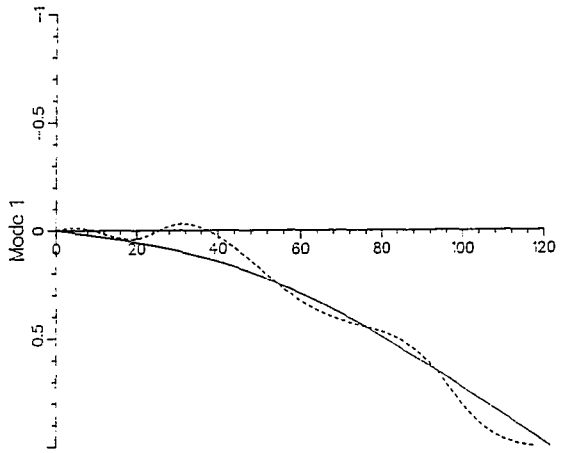

Fig. 7.1 First mode shape of lower link

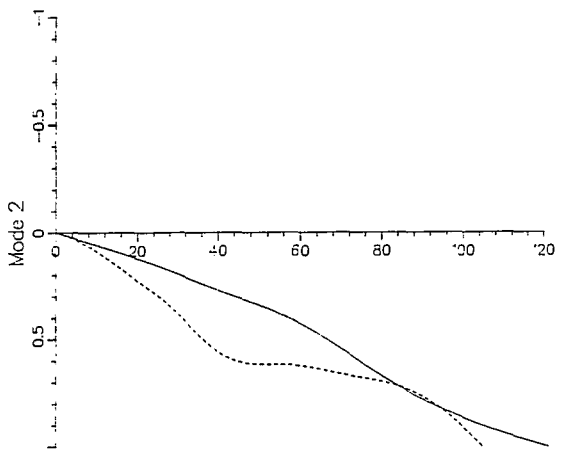

Fig. 7.2 Second mode shape of lower link

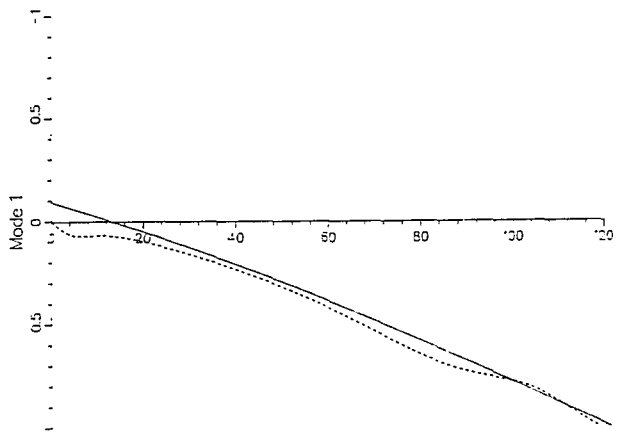

Fig. 7.3 First mode shape of upper link

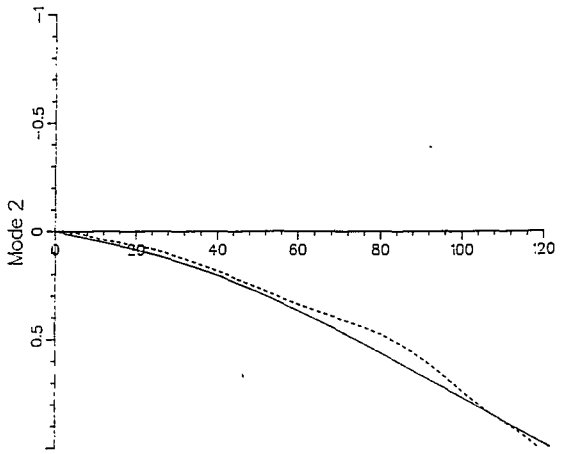

Fig. 7.4 Second mode shape of upper link

Table 7.1 Comparison of modal frequencies (Hz) of RALF without actuators attached

Mode	Experiment	Finite element
1	6.37	5.95
2	12.00	12.78
3	37.87	30.19
4	57.37	60.60
5	94.02	95.05

Table 7.2 Comparison of structural frequencies (Hz, with actuators attached)

Mode	Experiment	Finite element
1	5.70	6.08
2	9.12	9.12
3	30.00	29.70
4		49.50

Table 7.3 Comparison of structural frequencies (Hz, with actuators attached)

Mode	Experiment	Finite element
1	5.70	5.82
2	9.12	9.18
3	30.00	
4		55.70

When the linear hydraulic actuators are attached to the structure, the clamped boundary condition used previously must be modified. However, the hydraulic spring rate can be thought of as a "dynamic" spring in some sense so that the boundary condition for the driving joint can be modeled as a concentrated spring with an equivalent stiffness. The results for natural frequencies are shown in Table 7.2.

The parallel linkage driving joint 2 can be treated precisely as a geometric constraint to the dynamic behavior. An approximate method is used here which yields accurate results and exhibits the versatility of the modeling approach. The simplifications are motivated conceptually and experimentally. Conceptually, one expects flexure of the first and parallel driving links to have minimal effect on the distance between their pinned ends. Deflection of these links can thus cause no rotation of link 2, as would happen in the serial link case. This decouples the deflection rotations of the two links. Deflection translations show simplified coupling when joint two is near a right angle. By choosing the transformation matrix that describes link 2 to be independent of link 1 rotations the effect of the parallel linkage is thus incorporated. The symbolic manipulation of the equations easily handles this non-standard form.

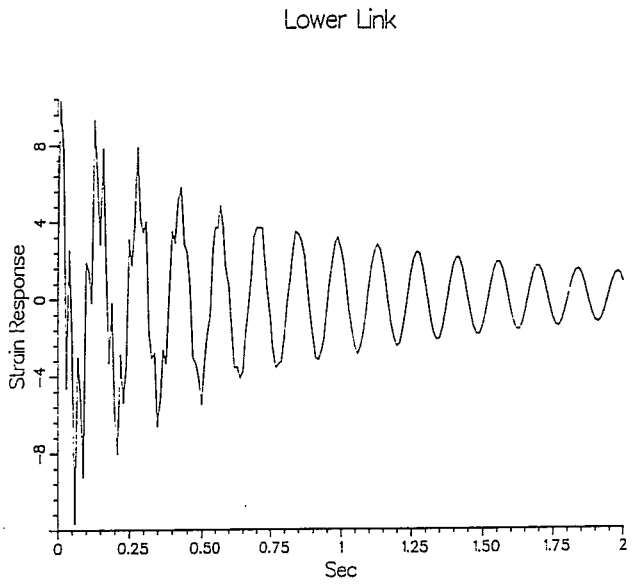

Fig. 7.7 Simulated strain response at the mid-point of lower link

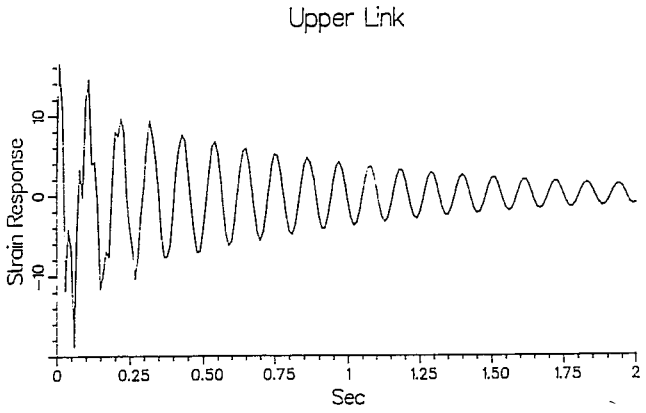

Fig. 7.8 Simulated strain response at the mid-point of upper link

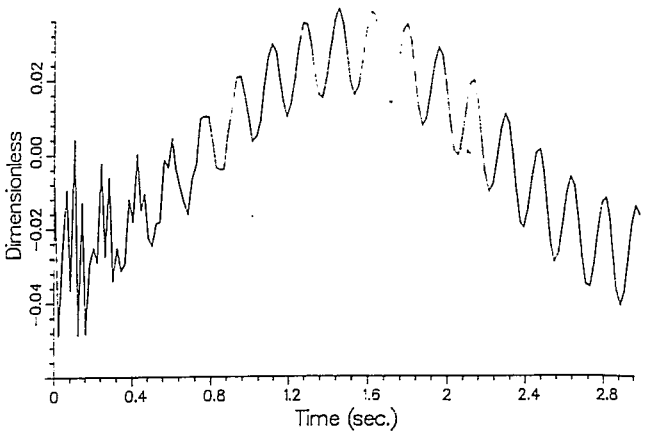

Fig. 7.9 Simulated strain response of lower link (sine wave)

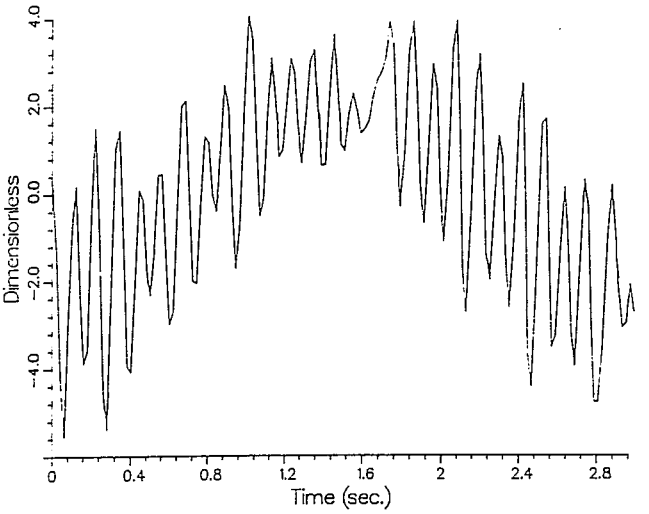

Fig. 7.10 Simulated strain response of upper link (sine wave)

each link arising from an impulsive force when the actuators are controlled. It is obvious that the structural damping should be included in the dynamics. From Figs. 7.5 and 7.6, the proportional damping ratio of about 0.2 is selected for use in the simulations. The Runge-Kutta method using sampling time 0.1 ms is utilized to solve the nonlinear dynamics. The results are shown in Figs. 7.7–7.8.

The responses from experiments and simulations show similar characteristics. A frequency of about 5.7 Hz for experiment and 6.1 Hz for simulation is most apparent in the lower link and a frequency of about 9.12 Hz for experiment and 9.18 Hz for simulation is most apparent in the upper link. Furthermore, the sine wave response can also be used to illustrate a property of the dynamic system. Figures 7.9 and 7.10 show the strain responses of simulations for the lower and upper links, while Figs. 7.11 and 7.12 show the experimental results. Further tuning of the model might improve the damping ratio of higher frequency modes. However, the fact that the simplified model used in the simulation may cause small deviation from measured experimental data is expected and acceptable from the engineering point of view.

VIII Summary and Conclusion

A transformation between two coordinates which includes rigid body motion and link deformation has been established in the form of a 4 × 4 matrix. Any point on the robotic arm can be described from the base coordinate in terms of those transformations. Due to the recursive nature of the transformation chain, the Lagrangian formulation of the dynamics is derived as efficiently as has been done in the rigid link case. The inertia matrix is shown to be positive and symmetric and a condition of skew-symmetry exists in the equations of motion that is useful in Lyapunov stability proofs (Yuan et al., 1989). There also exists a stiffness term in the equations, which is not present in the case of rigid-link manipulators. However, the approach requires that the link deflection is assumed to be small compared to joint motion and only rotational joints are allowed.

The system frequency deduced from the analytical formulation is highly dependent on the mode shapes of the link deflection, while the mode shapes are determined by the boundary conditions present. The application of feedback control to flexible manipulators also impacts the resultant flexible vibration modes. With the correct dynamical equation obtained in symbolic form, the choice of reasonable modes will result in the correct prediction of dynamic response. In the case of a one-link flexible manipulator, clamped-mass modes are selected when control action constrains the motion of the joint. The manipulator may have pinned-mass modes with no feedback control on the joint actuator (Cannon and Schmitz, 1984). RALF provides a more thorough and complicated case to verify the analysis. The dynamics of the actuator needs to be considered if the bandwidth of the actuator is not large enough to be ignored, i.e., the dynamics of the actuator with low bandwidth contributes to the boundary conditions. To elim-

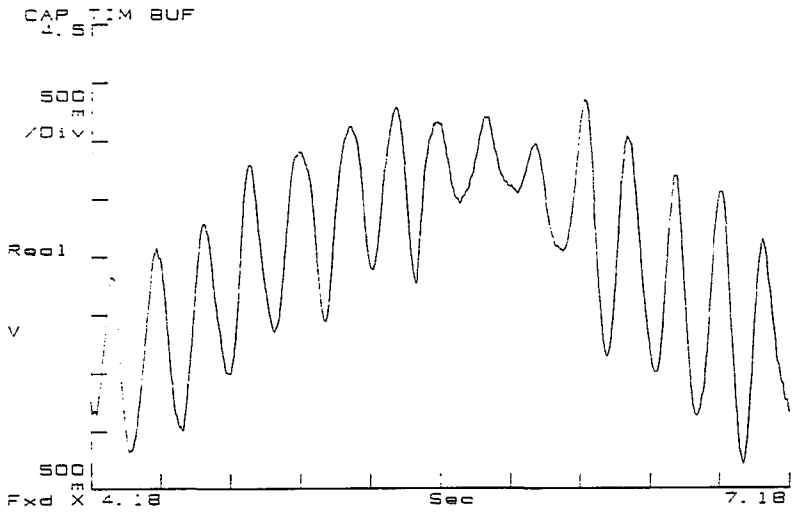

Fig. 7.11 Experimental strain response of lower link (sine wave)

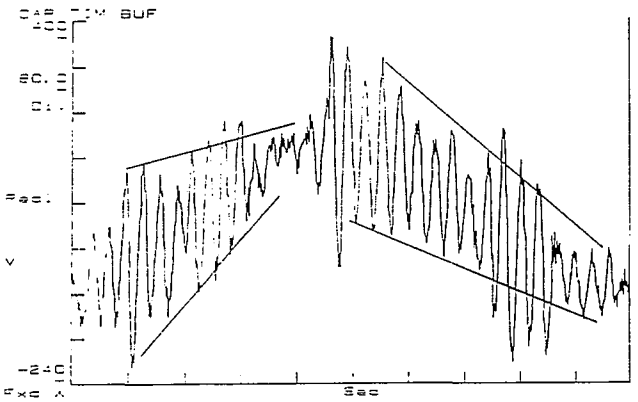

Fig. 7.12 Experimental strain response of upper link (sine wave)

inate the constraint force effect, the parallel driving link can be simplified as an equivalent spring and the kinematic constraints enforced through a modification of one matrix of the serial chain of transformation matrices. The kinematics affects the dynamics through the constraints that are enforced on the generalized coordinates. Mode shapes and joint transformations are the means for enforcing these constraints in the approach used here. The drive link dynamics have negligible coupling to the main links, serving principally to constrain link 2 to pure translation when link 1 is deforming (and no other coordinates are changing). This constraint can be enforced directly with the transformation matrix A_2.

The finite element method is used to derive suitable mode shapes without restriction on the design complexities experienced when shapes are analytically derived. With the experimental results and the numerical results, both frequency response and time response show reasonable agreement. While the comparisons between theory and experiment shown here are limited to small motions, the dynamic equations are compatible with large motions.

Acknowledgment

This work was partially supported by grant NAG-1-623 from the National Aeronautics and Space Administration.

References

Asada, H., and Slotine, J.-J. E., 1985, *Robot Analysis and Control*, John Wiley and Sons.

Bayo, E., 1987, "A Finite Element Approach to Control the End Point Motion of a Single-Link Flexible Robot," *Journal of Robotic Systems*, Vol. 4, pp. 63–75.

Book, W. J., 1974, "Modeling, Design and Control of Flexible Manipulator Arms," Ph.D. thesis, Cambridge, MA, Massachusetts Institute of Technology.

Book, W. J., 1979, "Analysis of Massless Elastic Chains with Servo Controlled Joints," ASME JOURNAL OF DYNAMIC SYSTEMS, MEASUREMENT, AND CONTROL, Vol. 101, pp. 187–192.

Book, W. J., 1984, "Recursive Lagrangian Dynamics of Flexible Manipulator Arms," *International Journal of Robotics Research*, Vol. 3, pp. 87–101.

Cannon, R. M., and Schmitz, E., 1984, "Initial Experiments on the End-point Control of a Flexible One-link Robot," *International Journal of Robotics Research*, Vol. 2, pp. 62–75.

Greenwood, D. J., 1965, *Principles of Dynamics*, Prentice Hall Inc.

Hastings, G. G., 1986, "Controlling Flexible Manipulators, an Experimental Investigation," Ph.D. thesis, Georgia Institute of Technology, Atlanta, GA.

Hastings, G. G., and Book, W. J., 1987, "A Linear Dynamic Model for Flexible Robotic Manipulators," *IEEE Control Systems Magazine*, Vol. 7, pp.61–64.

Hollerbach, J. M., 1980, "A Recursive Lagrangian Formulation of Manipulator Dynamics and a Comparative Study of Dynamics Formulation Complexity," *Transactions on System, Man, and Cybernetics*, Vol. SMC-10, pp. 730–736.

Huggins, J. D., 1988, "Experimental Verification of a Model of a Two-Link Flexible, Lightweight Manipulator," M.S. thesis, Georgia Institute of Technology, Atlanta, GA.

Kane, T. R., and Levinson, 1985, *Dynamics, Theory and Application*, McGraw-Hill.

Maizza-Neto, O., 1974, "Modal Analysis and Control of Flexible Manipulator Arms," Ph.D. thesis, Massachusetts Institute of Technology, Cambridge, MA.

Meirovitch, L., 1967, *Analytical Methods in Vibrations*, The Macmillan Co., New York.

Merritt, H. E., 1967, *Hydraulic Control Systems*, John Wiley and Sons.

Oakley, C. M., and Cannon, R. H., 1989, "Equations of Motion for an Experimental Planar Two-link Flexible Manipulator," ASME DSC-Vol. 14.

Paul, R. P., *Robot Manipulators*, MIT Press.

Spong, M. W., 1987, "Modeling and Control of Elastic Joint Robots," ASME JOURNAL OF DYNAMIC SYSTEMS, MEASUREMENT, AND CONTROL, Vol. 109, pp. 310–319.

Yuan, B.-S., Book, W. J., and Huggins, J. D., 1989, "Decentralized Adaptive Control of a Two Degree of Freedom Flexible Arm," ASME, DSC-Vol. 14.

Yuan, B.-S., Book, W. J., and Siciliano, B., 1989, "Direct Adaptive Control of a One-Link Flexible Arm with Tracking," *Journal Robotic Systems*, Vol. 6, pp. 663–680.

APPENDIX A

From Eq. (2.6), r_i can also be represented as (Yuan et al., 1989)

$$\dot{r}_i = J_i \dot{x}_i \tag{A.1}$$

where

L_i is the total number of generalized coordinates

J_i is $4 \times L_i$ of Jacobian matrix

x_i is the time derivative vector including i joints, say q_1, q_2, . . . , q_i and $(L_i - i)$ time dependent flexible coordinates.

The kinetic energy of the n-link flexible arm is then

$$KE = \frac{1}{2}\sum_{i=1}^{n}\int_{\text{link}_i} \dot{r}_i^T \dot{r}_i dm$$

$$= \frac{1}{2}\dot{x}^T M \dot{x} \tag{A.2a}$$

where

$$M = \sum_{i=1}^{n}\int_{\text{link}_i} [J_i^T J_i] dm \tag{A.2b}$$

Obviously, the inertia matrix M is positive and symmetric in (A.2b) and in (2.10a). The kinetic energy in (2.10a) can be expressed by physical reasoning. The necessary and sufficient conditions for this are that the inertia matrix satisfies positive definiteness, unless the system is at rest.

The coupling element of C which represents the coefficient in the second term in (4.6a) has the following relation:

$$\sum_{i=1}^{n}\sum_{j=0}^{m_i}\sum_{\alpha=1}^{n}\sum_{\beta=0}^{m_\alpha}\left(\frac{\partial m_{ijpq}}{\partial x_{\alpha\beta}} - \frac{1}{2}\frac{m_{ij\alpha\beta}}{\partial \dot{x}_{pq}}\right)\dot{x}_{ij}\dot{x}_{\alpha\beta}$$

$$= \frac{1}{2}\sum_{i=1}^{n}\sum_{j=0}^{m_i}\left\{\sum_{\alpha=1}^{n}\sum_{\beta=0}^{m_\alpha}\frac{\partial m_{ijpq}}{\partial x_{\alpha\beta}}\dot{x}_{\alpha\beta} + \sum_{\alpha=1}^{n}\sum_{\beta=0}^{m_\alpha}\left(\frac{\partial m_{\alpha\beta pq}}{\partial x_{ij}} - \frac{\partial m_{\alpha\beta ij}}{\partial x_{pq}}\right)\dot{x}_{\alpha\beta}\right\}\dot{x}_{ij} \tag{A.3}$$

In comparison with (4.7) and defining the element of the coupling matrix H and $[H_{ijpq}]$, we have

$$[H_{ijpq}] = \frac{1}{2}\sum_{\alpha=1}^{n}\sum_{\beta=0}^{m_\alpha}\frac{\partial m_{ijpq}}{\partial x_{\alpha\beta}}\dot{x}_{\alpha\beta} + \frac{1}{2}\sum_{\alpha=1}^{n}\sum_{\beta=0}^{m_\alpha}\left(\frac{\partial m_{\alpha\beta pq}}{\partial x_{ij}} - \frac{\partial m_{\alpha\beta ij}}{\partial x_{pq}}\right)\dot{x}_{\alpha\beta}$$

$$= \frac{1}{2}[m_{ijpq}] + \frac{1}{2}\sum_{\alpha=1}^{n}\sum_{\beta=0}^{m_\alpha}\left(\frac{\partial m_{\alpha\beta pq}}{\partial x_{ij}} - \frac{\partial m_{\alpha\beta ij}}{\partial x_{pq}}\right)\dot{x}_{\alpha\beta} \tag{A.4}$$

Defining W = $\dot{M}$-2H, the above (A.4) gives

$$W_{ijpq} = \sum_{\alpha=1}^{n}\sum_{\beta=0}^{m_\alpha}\left(\frac{\partial m_{\alpha\beta pq}}{\partial x_{ij}} - \frac{\partial m_{\alpha\beta pq}}{\partial x_{pq}}\right)\dot{x}_{\alpha\beta} = -W_{pqij} \tag{A.5}$$

This shows that ($\dot{M}$-2H) is skew-symmetric; i.e., $W + W^T = 0$. By setting $m_\alpha = 0$ in (A.3), it becomes the case of rigid robotic arms, which was found in reference (Asada and Slotine, 1985).

APPENDIX B

Independent linear controllers at each joint, commonly called joint proportional-derivative (PD) controllers, which are based on the local measurements of joint positions (q_i) and velocities ($\dot{q}_i$) are described as follows:

$$\tau_i = -K_{pi}\tilde{q}_i - K_{Di}\dot{\tilde{q}}_i \tag{B.1}$$

where

τ_i is the torque acting on the ith joint.

K_{pi} and K_{Di} are positive constants. $\tilde{q}_i = q_i - q_{ri}$ and $\dot{\tilde{q}} = \dot{q}_i - \dot{q}_{ri}$, ($\tilde{q} = \dot{q}_i$),

while q_{ri} is the reference state and assumed to be constant. Physically, the feedback system effectively equips each joint with equivalent rotary spring and damper. The frequency domain approach has been taken with the linearized system in previous work (Book, 1974). A Lyapunov approach is applied here to show the resulting stability.

First, the following equality (nonconservative forces) exists,

$$\dot{X}^T Q = \dot{q}^T \tau \tag{B.2}$$

where X, Q are given in (4.7). $q^T = [q_1, q_2, \ldots q_n]$ represents the joint coordinates in (4.7). $\tau = [\tau_1, \tau_2, \ldots \tau_n]^T$ and $\tau_i = Q_{i0}$.

Consider a Lyapunov candidate V associated with the total mechanical energy of the feedback system:

$$V = \frac{1}{2}[\dot{X}^T M \dot{X} + \overline{X}^T K \overline{X} + \tilde{q}^T K_p \tilde{q}] \tag{B.3}$$

where K_p = diag[K_{pi}] and K is the positive stiffness as well as time independent matrix as (4.7). Note that K is derived from link strain potential energy which is composed of the quadratic form of the mode shape (Section 3.3).

Differentiating V with respect to time gives,

$$\dot{V} = \dot{\tilde{q}}^T K_p \tilde{q} + \dot{X}^T M \ddot{X} + \frac{1}{2}\dot{X}^T \dot{M} \dot{X} + \dot{X}^T K \overline{X}$$

$$= \dot{\tilde{q}}^T K_p \tilde{q} + \dot{X}^T (M\ddot{X} + K\overline{X}) + \frac{1}{2}\dot{X}^T \dot{M} \dot{X} \tag{B.4}$$

Note that $\dot{X} = \dot{\overline{X}}$. By substituting (B.1), (B.2), (4.7), and ($\dot{M}$-2H) into above

$$\dot{V} = \dot{\tilde{q}}^T K_p \tilde{q} + \dot{X}^T (Q - H\dot{X}) + \frac{1}{2}\dot{X}^T \dot{M} \dot{X}$$

$$= \dot{\tilde{q}}^T K_p \tilde{q} + \dot{X}^T Q + \frac{1}{2}\dot{X}^T (\dot{M} - 2H)\dot{X}$$

$$= \dot{\tilde{q}}^T K_p \tilde{q} + \dot{q}^T \tau$$

$$= -\dot{q}^T K_D \dot{q} \leq 0$$

where K_D = diag[K_{pi}] is a positive matrix.

Therefore, the linearized system with joint PD controller is stable.